



Analysis of angular dispersion induced by wavefront rotation in nanosecond optical parametric chirped pulse amplification

YEONG GYU KIM,^{1,2} HWANG WOON LEE,¹  HAN BUM IM,¹ JI IN KIM,^{1,2} JAE HEE SUNG,^{1,3} JIN WOO YOON,^{1,3} SEONG KU LEE,^{1,3,4} AND CHANG HEE NAM^{1,2,5} 

¹Center for Relativistic Laser Science, Institute for Basic Science, Gwangju 61005, Republic of Korea

²Department of Physics and Photon Science, Gwangju Institute of Science and Technology, Gwangju 61005, Republic of Korea

³Advanced Photonics Research Institute, Gwangju Institute of Science and Technology, Gwangju 61005, Republic of Korea

⁴lsk@gist.ac.kr

⁵chnam@gist.ac.kr

Abstract: Angular dispersion observed in a nanosecond optical parametric chirped-pulse amplification (ns-OPCPA) amplifier adopted in the frontend of a multi-PW laser was analyzed. The theory on the angular dispersion, extended by including the wavefront rotation and the pulse front tilt of a strongly chirped laser pulse, revealed that the wavefront rotation is a major contributor to the angular dispersion, as compared to the pulse front tilt, in a ns-OPCPA amplifier. It was also shown that the wavefront rotation could be introduced by the phase mismatch and the noncollinear propagation angle in the noncollinear ns-OPCPA amplifier. The theoretical prediction was experimentally verified by measuring the angular dispersion of the ns-OPCPA frontend installed in the 20-fs, 4-PW Ti:Sapphire laser. We emphasize the importance of the proper characterization and control of the angular dispersion in the ns-OPCPA amplifier since the focus intensity of an ultrahigh power laser could be significantly reduced due to the spatiotemporal effect even for small induced angular dispersion.

© 2020 Optical Society of America under the terms of the [OSA Open Access Publishing Agreement](#)

1. Introduction

Since the invention of the chirped pulse amplification technique [1], ultrahigh power lasers have been developed [2,3] and applied intensively for the investigations of strong-field physics [4,5]. The first ultrahigh power laser exceeding an output power of 1 PW was demonstrated using an Nd:Glass laser with a pulse duration of 0.5 ps at Lawrence Livermore National Laboratory [6]. The technical advancement of high power femtosecond lasers prompted the development of a 33 fs, 0.85 PW Ti:Sapphire laser in Japan Atomic Energy Research Institute [7], and then a 30 fs, 1.0 PW laser at Advanced Photonics Research Institute [8]. A further development utilizing the broad gain bandwidth of Ti:Sapphire has prompted the development of a 20 fs, 4 PW laser at the Center for Relativistic Laser Science in 2017 [2]. In this case, an optical parametric chirped-pulse amplification (OPCPA) stage was employed in the frontend part [9]. Because of the use of a strongly chirped ns pulse, we carried out the systematic analysis of angular dispersion in the OPCPA process.

An OPCPA amplifier offers advantages in developing ultrashort high-power lasers [10]. The nonlinear process between signal and pump beams can enhance the temporal contrast between prepulses and the main ultrashort high-power pulse [11,12], and the low thermal load to nonlinear crystals used in an OPCPA amplifier chain is beneficial for repetitive laser operation [13,14]. In addition, the broadband gain through noncollinear phase-matching enables the amplification of

ultrashort pulses [15], which allows to avoid the gain narrowing accompanied in a very high gain amplification frontend stage of a CPA laser [10]. The OPCPA amplifier has been, thus, adopted frequently in the frontend of ultrahigh power lasers [16–20].

However, the OPCPA amplifier with a noncollinear geometry may induce angular dispersion - the angular spread of the propagation direction for different spectral components of a laser pulse [21]. From the theory on the spatiotemporal coupling (STC) of a laser pulse, it is known that angular dispersion can be generated by pulse front tilt and wavefront rotation [22,23]. And this angular dispersion can affect the focal spot size and pulse width [24]. In the case of OPCPA amplifiers using ps chirped pulses, there are studies on the beam quality degradation due to angular dispersion caused by the pulse front tilt [21,25–27]. On the other hand, in the case of OPCPA amplifiers using ns chirped pulses, studies have been conducted mainly on amplification characteristics [20,28,29]. Consequently, it is crucial to investigate the angular dispersion of the ns-OPCPA amplifier used as the frontend of ultrahigh power lasers.

In this paper, we report the analysis of the angular dispersion induced in the ns-OPCPA amplifier. In Sec. 2, the angular dispersion due to pulse front tilt and wavefront rotation is theoretically derived and applied to the ns-OPCPA amplifier. In Sec. 3, the experimental proof for the analytical theory is presented by measuring the angular dispersion of the ns-OPCPA amplifier, and its effect on the focal spot parameters is shown. The method to compensate for the angular dispersion is discussed in Sec. 4. The conclusion is given in Sec. 5.

2. Theory

The angular dispersion usually appears when a laser pulse passes through a dispersive media, for example, prism and diffraction grating [30]. Besides, the angular dispersion can be induced when the laser pulse experiences a nonlinear process. An example of such a nonlinear process is produced by the pulse front tilt, which is raised by a geometry of the noncollinear OPA amplifier [21], where the magnitude of induced angular dispersion would be the same as that of the pulse front tilt if the laser pulse does not possess temporal chirp [31]. Although a spatiotemporal theory handled the first-order term of the spatiotemporal couplings analytically [22], it enabled us to understand the relation between the angular dispersion and other various laser parameters. This theory, applied to the case of the OPCPA amplifier, shows that even with the same pulse front tilt, the angular dispersion decreases with the increase of pulse width due to the temporal chirp [27].

Although the previous study enhanced the understanding of the generation of the angular dispersion in the OPCPA amplifier, the systematic analysis of the effect of the wavefront rotation on the angular dispersion has not been properly done.

In Sec. 2.1, the theory of the angular dispersion generation is generalized by including the wavefront rotation. In Sec. 2.2, we show how the wavefront rotation can occur in the ns-OPCPA amplifier. In Sec. 2.1 and Sec. 2.2, the pulse front tilt and the wavefront rotation appear as the real and the imaginary parts of the first-order spatiotemporal coupling in the x - t domain, respectively. Finally, in Sec. 2.3, the angular dispersion is derived for a broadband laser pulse without the Taylor expansion for the case that a signal pulse has a large temporal chirp.

2.1. Main contributors to angular dispersion

Main contributors to angular dispersion were analyzed by using the first-order space-time theory. Suppose a laser pulse has a time-dependent rotation of wavefront angle $\theta(t)$, i.e., wavefront rotation, a spatiotemporal phase function of the laser pulse, $R(x, t)$ is

$$R(x, t) = k \sin[\theta]x = k(\sin[\theta(t=0)] + \delta\theta)x, \quad (1)$$

where k is a wavevector, t is the retarded time in the pulse frame, and $\delta\theta$ is a Taylor expansion of the phase function. Assumed that the expansion of the phase function can be terminated after the

linear term, that is

$$\delta\theta = \left. \frac{d \sin[\theta(t)]}{dt} \right|_{t=0} t. \quad (2)$$

If the wavefront angle is zero at $t = 0$, the spatiotemporal phase function with a wavefront rotation parameter γ is

$$R(x, t) \cong k\delta\theta x = k \left. \frac{d \sin[\theta(t)]}{dt} \right|_{t=0} xt = \gamma xt. \quad (3)$$

The temporal phase function of the laser pulse is

$$\varphi_t(t) = -\omega_c t - \beta t^2. \quad (4)$$

where ω_c is a carrier frequency and β is a temporal chirp parameter. With the first-order expansion of the spatiotemporal phase function and the temporal phase function, the laser electric field can be expressed as

$$\begin{aligned} E(x, t) &= |E(x, t)| \exp[i\varphi_t(t) + iR(x, t)] \\ &= \exp \left[-\left(\frac{x}{w_0}\right)^2 - \left(\frac{t-\Gamma x}{\tau}\right)^2 \right] \exp[i(\gamma xt - \omega_c t - \beta t^2)]. \end{aligned} \quad (5)$$

with the beam size w_0 , the pulse width τ , the pulse front tilt $\Gamma = dt_0/dx$, and t_0 is the pulse front.

To transform the envelope of the laser electric field from the x - t domain to the ω - k domain for obtaining the angular dispersion, the temporal and spatial Fourier transform was performed on Eq. (5).

$$\begin{aligned} A(k_x, \omega) &= \text{FT}_t[\text{FT}_x[A(x, t)]] \\ &= \frac{1}{\sqrt{\frac{1}{\tau^2} + i\beta} \sqrt{\frac{C_1}{w_0^2 \beta \tau^2 - i\omega_0^2}}} \\ &\times \exp \left[\frac{w_0^2(i-\beta\tau^2)k_x^2 + w_0^2(-2i\Gamma + \gamma\tau^2)k_x\omega + i(\tau^2 + \Gamma^2 w_0^2)\omega^2}{4\beta\tau^2 + w_0^2(4\beta\Gamma^2 - i\gamma^2\tau^2 - 4\gamma\Gamma) - 4i} \right]. \end{aligned} \quad (6)$$

where FT_x is the spatial Fourier transform, FT_t is the temporal Fourier transform, and spatiotemporal envelope $A(x, t) = E(x, t) \exp[i\omega_c t]$.

For the clarification, Eq. (6) may be rewritten by substituting the variables as

$$\begin{aligned} A(k_x, \omega) &= H\Omega(\omega)K \left(k_x - \frac{dk_c}{d\omega} \omega \right) \exp[i\varphi(k_x, \omega)], \\ H &= \frac{1}{\sqrt{\frac{1}{\tau^2} + i\beta} \sqrt{\frac{C_1}{w_0^2 \beta \tau^2 - i\omega_0^2}}}, \\ \Omega(\omega) &= \exp[-C_2(\gamma^2\tau^2 w_0^2 + 4)(\tau^2 + \Gamma^2 w_0^2)\omega^2], \\ K \left(k_x - \frac{dk_c}{d\omega} \omega \right) &= \exp \left[-C_2 \left(k_x - \frac{dk_c}{d\omega} \omega \right)^2 \right], \\ \varphi(k_x, \omega) &= \angle A - \angle H, \end{aligned} \quad (7)$$

with the following auxiliary variables, where \angle is the argument of the complex number.

$$\begin{aligned} C_1 &= 4\beta\tau^2 + w_0^2(4\beta\Gamma^2 - i\gamma^2\tau^2 - 4\gamma\Gamma) - 4i, \\ C_2 &= \frac{1}{C_1 C_1^*}, \\ \frac{dk_c}{d\omega} &= \frac{2\beta\gamma\tau^4 - \gamma w_0^2(\gamma - 2\beta\Gamma)\tau^2 + 4\Gamma}{4\beta^2\tau^4 + w_0^2(\gamma - 2\beta\Gamma)^2\tau^2 + 4}. \end{aligned} \quad (8)$$

In Eq. (7), the complex function H is a constant for a given input condition, and the coupled phase function $\varphi(k_x, \omega)$ does not influence the envelope of the laser pulse in the Fourier domain

(ω - k domain). The spectrum function $\Omega(\omega)$ can be ignored because, even if it contributes to the spectral shape, it does not contain coupling terms. As a consequence, for calculating the angular dispersion, we focus on the coupled amplitude function $K(k_x, (dk_c/d\omega)\omega)$ and express the angular dispersion in terms of the coupling parameter $dk_c/d\omega$ in Eq. (8).

Equation (8) shows that the angular dispersion can be affected by both pulse front tilt and wavefront rotation. For the estimation of the angular dispersion, the following two cases are considered. (1) A chirp-free femtosecond pulse is amplified in an OPA amplifier. (2) All parameters are the same as those of case (1), except that the femtosecond signal pulse is stretched to several nanoseconds. In case (1), the τ^2 and the τ^4 terms are much smaller than the constant term, and then the angular dispersion $dk_c/d\omega$ can be expressed as

$$\frac{dk_c}{d\omega} = \Gamma. \quad (9)$$

This result indicates that the angular dispersion equals the pulse front tilt, agreeing with the previous results [21,26,27]. On the other hand, in case (2), the terms with τ^4 are much larger than others. The angular dispersion $dk_c/d\omega$ can, thus, be expressed as

$$\frac{dk_c}{d\omega} = \frac{\gamma}{2\beta}. \quad (10)$$

Equation (10) means that, for a highly stretched signal pulse, the angular dispersion is determined mainly by the wavefront rotation and the temporal chirp, although the angular dispersion is affected by many parameters. In the process of inducing the angular dispersion, the temporal chirp acts like a rocker switch that determines the main contributor to the angular dispersion.

2.2. Generation of a wavefront rotation in the ns-OPCPA amplifier

In order to apply the result on the angular dispersion in Sec. 2.1 to the case of a ns-OPCPA amplifier, the wavefront rotation induced by the ns-OPCPA amplifier is analyzed. In the ns-OPCPA amplifier, the relation between instantaneous frequencies of the three interacting pulses is [32]

$$\omega_p(t) = \omega_s(t) + \omega_i(t), \quad (11)$$

where instantaneous frequency $\omega_s(t) = \omega_s + 2\beta t$, $\omega_i(t) = \omega_i - 2\beta t$, and $\omega_p(t) = \omega_p$. Then, a phase mismatch is a function of the instantaneous frequencies

$$\Delta \vec{k}(t) = \vec{k}_p[\omega_p(t)] - \vec{k}_s[\omega_s(t)] - \vec{k}_i[\omega_i(t)]. \quad (12)$$

The coupled equations for describing the optical parametric process of the signal and the idler are expressed as follows:

$$\begin{aligned} \frac{dA_s}{dz} &= i \frac{\omega_s^2(t) d_{\text{eff}} A_p}{k_s[\omega_s(t)] c^2} A_i^* \exp[i\Delta k(t)z], \\ \frac{dA_i}{dz} &= i \frac{\omega_i^2(t) d_{\text{eff}} A_p}{k_i[\omega_i(t)] c^2} A_s^* \exp[i\Delta k(t)z], \end{aligned} \quad (13)$$

where A_s , A_i , and A_p are the electric field of the signal, the idler, and the pump, respectively [33,34]. In Eq. (13), d_{eff} is the effective nonlinear optical coefficient, k_s , k_i , and k_p are the wavevector of the signal, the idler, and the pump, respectively, and $\Delta k = |\Delta \vec{k}|$ is the scalar phase mismatch. In the case of the broadband ns-OPCPA using a positively chirped laser pulse, the phase mismatch changes in time within the ns-pulse duration because the instantaneous wavelength component varies from long wavelength to short wavelength with time. Since the beam size is large enough and the pulse width is sufficiently long in the ns-OPCPA amplifier, the diffraction effect and

group velocity dispersion is ignored in Eq. (13). Assuming an undepleted pump with high gain, $g \gg 1$, and plane wave, the phases of signal and idler at distance z can be expressed as

$$\begin{aligned}\varphi_s(t) &= \frac{\Delta k(t)}{2} \left(z + \frac{1}{g} \frac{\exp[gz] - \exp[-gz]}{\exp[gz] + \exp[-gz]} \right) \cong \frac{\Delta k(t)z}{2}, \\ \varphi_i(t) &= \frac{\Delta k(t)}{2} \left(z + \frac{1}{g} \frac{\exp[gz] - \exp[-gz]}{\exp[gz] + \exp[-gz]} \right) + \frac{\pi}{2} \cong \frac{\Delta k(t)z + \pi}{2},\end{aligned}\quad (14)$$

where gain $g = \sqrt{\omega_s^2 \omega_i^2 d_{\text{eff}}^2 A_p^2 / k_s k_i c^4 - \Delta k^2 / 4}$.

The geometry of the noncollinear propagation of the signal and the idler beam is shown in Fig. 1(a). In the OPCPA amplifier with tangential phase-matching, adopted to avoid the parasitic second harmonic generation that decreases the OPCPA efficiency [35], the signal beam moves away from the pump and the idler beams, while the pump and the idler beams propagate together. To simplify a theoretical model, it is assumed that the crystal length is sufficiently long enough to separate the signal beam from the pump beam, and the slight deviation of the pump beam to the idler beam is neglected. While the signal beam becomes spatially separated from the pump beam, the idler beam coupled with the pump beam produces the signal beam through the difference frequency generation (DFG) process. Hence, the signal beam consists of two parts - the amplified signal beam (red) by the OPA process and the signal beam (blue) generated by the DFG process in Fig. 1(b).

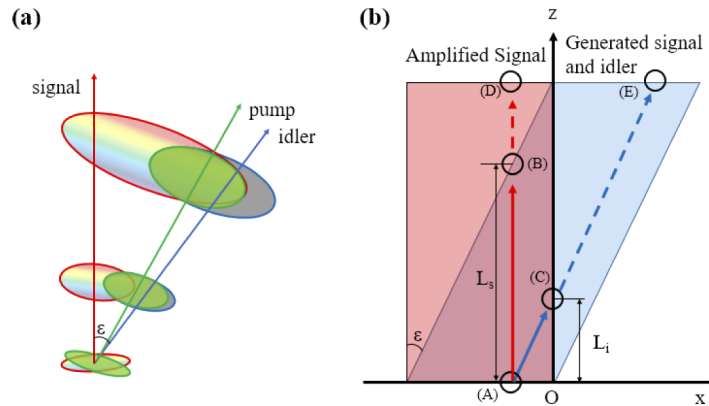


Fig. 1. (a) The schematic of the tangential phase matching in the noncollinear optical parametric amplifier. As the signal beam propagates through a nonlinear crystal, it is separated from the pump and idler beam. (b) Generation of the signal and idler beam. The signal beam consists of an amplified signal beam (red) and a generated signal beam (blue) from DFG process. The propagation path of the signal and idler beam, starting at point (A), are plotted as the red (signal) and the blue (idler) solid arrows, respectively. Before reaching point (B) or (C), the signal and idler beam are overlapped with each other. After the signal and idler beam pass through point (B) or (C), two beams are completely separated. From point (B) or (C) to the end of the crystal (D) or (E), the propagation paths are plotted as dotted arrows. The effective interaction lengths of the signal and idler beam are defined as L_s and L_i , respectively.

To obtain the phase of the signal beam by the OPA and DFG process, first, the phase of the signal beam amplified by the OPA process was derived. By taking the imaginary part of equations under the polar form, $A = a \exp(i\varphi)$, the phase change between amplitudes with respect to z can be expressed as following relation [34]

$$\frac{d\varphi_{s,i}}{dz} \propto \frac{a_{i,s}}{a_{s,i}}. \quad (15)$$

From Eq. (15), it is noted that the phase of the signal beam does not change significantly when the idler beam amplitude a_i is much smaller than the signal beam amplitude a_s . In Fig. 1(b), the signal and idler beam propagate along the red arrows and the blue arrows, respectively. The signal beam at point (A) ($x = x_0, z = 0$), propagates along the red solid arrow and amplified by optical parametric process before point (B). The x, y coordinates of point (B) are given by

$$B(x, z) = \left(x_0, L + \frac{x}{\tan \varepsilon} \right), \quad (16)$$

where L is the crystal length and ε is the noncollinear propagation angle between the signal and idler beam. At the point (B) in Fig. 1(b), the signal and idler beam are fully deviated and after this point, plotted as the red dashed arrow, the phase of the signal beam barely changes according to Eq. (15). Thus, the phase of the signal beam at point (D) is approximately equal to that of the signal beam at point (B)

$$\phi_s(x \leq 0, t, z) \cong \varphi_s(t, L_s), \quad (17)$$

where L_s is the effective interaction length and it equals to z coordinate of point (B) $L + x/\tan \varepsilon$. From Eqs. (14)-(17), the phase of the amplified signal by the OPA process can be obtained,

$$\phi_s(x \leq 0, t, z) = \frac{\Delta k(t)}{2} \left(z + \frac{x}{\tan \varepsilon} \right). \quad (18)$$

From now, we focus on the phase of the idler beam to obtain the phase of the signal beam by the DFG process. The idler beam generated at point (A) propagates along the blue solid arrows. At point (C), the idler beam is deviated from the amplified signal beam. The x, y coordinates of point (C) are given by

$$C(x, z) = \left(0, -\frac{x_0}{\tan \varepsilon} \right). \quad (19)$$

Along the path from (C) to (E), plotted as the blue dashed arrow, the phase of the idler beam barely changes according to Eq. (15). Thus, the phase of the idler beam at point (E) is approximately equal to that of the idler beam at point (C)

$$L_i \quad (20)$$

where $\phi_i(x, t, z) \cong \varphi_i(t, L_i)$, is the effective interaction length of the idler beam and it equals to the z coordinate of point (C), $z - x/\tan \varepsilon$. Then, the phase of the idler beam can be derived from Eqs. (14) and (20).

$$\phi_i(x > 0, t, z) = \frac{\Delta k(t)}{2} \left(z - \frac{x}{\tan \varepsilon} \right) + \frac{\pi}{2}. \quad (21)$$

By taking the imaginary part of Eq. (13), the phase equation of the signal beam by the DFG process can be expressed as

$$\phi_s(x > 0, t, z) = \Delta k(t)z - \phi_i(x, t) + \frac{\pi}{2}. \quad (22)$$

Using the phase of the idler beam, Eq. (21), and the above phase equation Eq. (22), the phase of the signal beam by the DFG is

$$\phi_s(x > 0, t, z) = \frac{\Delta k(t)}{2} \left(z + \frac{x}{\tan \varepsilon} \right). \quad (23)$$

Equations (18) and (23), the phases of the amplified signals by the OPA and the DFG process, are the same form. Accordingly, the phase functions of the entire signal beams can be written as

$$\phi_s(x, t, z) = \frac{\Delta k(t)}{2} \left(z + \frac{x}{\tan \varepsilon} \right). \quad (24)$$

Then, the phase mismatch can be approximated using the Taylor expansion.

$$\begin{aligned}\Delta k(t) &= \Delta k + \delta k, \\ \delta k &= \left. \frac{d\Delta k}{dt} \right|_{t=0} t + \frac{1}{2} \left. \frac{d^2\Delta k}{dt^2} \right|_{t=0} t^2 + \dots,\end{aligned}\quad (25)$$

where the time $t = 0$ is defined for the moment of the central wavelength at 800 nm, and Δk_0 is the phase mismatch at $t = 0$. The phase mismatch can be expressed with the first-order term as

$$\Delta k(t) \cong \left. \frac{d\Delta k}{dt} \right|_{t=0} t. \quad (26)$$

With Eqs. (24) and (26), the spatiotemporal phase of the signal beam can be expressed as

$$A(x, t) \propto |A(x, t)| \exp \left[i \frac{1}{2 \tan \varepsilon} \left. \frac{d\Delta k}{dt} \right|_{t=0} xt \right]. \quad (27)$$

From Eqs. (5) and (27), the imaginary spatiotemporal coupling term γ , the wavefront rotation, can be determined by

$$\gamma = \frac{1}{2 \tan \varepsilon} \left. \frac{d\Delta k}{dt} \right|_{t=0}. \quad (28)$$

Because it is assumed that the signal beam has a large temporal chirp, the angular dispersion is obtained by inserting the spatiotemporal coupling term γ in Eq. (28) to Eq. (10):

$$\frac{dk_c}{d\omega} = \frac{1}{4\beta \tan \varepsilon} \left. \frac{d\Delta k}{dt} \right|_{t=0}. \quad (29)$$

According to this theory, the phase of the signal beam is distorted due to phase mismatch with walk-off, which introduces the wavefront rotation to the signal beam. Consequently, the wavefront rotation leads to the angular dispersion in the ns-OPCPA amplifier.

2.3. Angular dispersion for broadband laser pulses in the ns-OPCPA amplifier

Equation (29) represents the angular dispersion near the center wavelength in the ns-OPCPA amplifier, but it cannot describe the angular dispersion of the broadband pulse, because the first-order expression is insufficient to express the phase mismatch of the broadband pulse. Here, we derived the angular dispersion of the broadband pulse in the ns-OPCPA amplifier. The broadband laser pulse with time-dependent phase mismatch in the x-t domain is expressed as

$$A(x, t) = \exp \left[- \left(\frac{t - \Gamma x}{\tau} \right)^2 - \left(\frac{x}{w_0} \right)^2 \right] \exp \left[\frac{i\Delta k(\omega(t))x}{2 \tan \varepsilon(\omega(t))} \right] \exp[-i\beta t^2]. \quad (30)$$

To characterize the angular dispersion of the broadband laser pulse in the OPCPA amplifier, the laser electric field Eq. (30) was transformed numerically to the ω -k domain. The parameters in the calculation were similar to the experimental conditions except for the temporal chirp and pulse width: radius $(1/e^2)$ $w_0 = 2.45$ mm, induced pulse front tilt [26] $\Gamma = \tan(\alpha)/v_g = 232$ fs/mm where group velocity v_g , temporal chirp $1/\beta = 100,000$ fs², and pulse width $\tau = 5,800$

In order to avoid the huge memory required for numerically treating the ns laser pulse, the temporal chirp and pulse duration were intentionally reduced; the actual temporal chirp and pulse width in the experiment was about 100 times larger than the above values used in the calculation. The phase mismatch Δk and the crossing angle ε were calculated with the phase-matching condition: $\alpha = 2.369^\circ$, $\theta = 23.894^\circ$, $\varepsilon = 7.118^\circ$, and $\Delta k(\lambda = 765\text{nm}) = 0$. The envelopes of the laser pulse in the x-t domain and the ω -k domain are shown in Fig. 2(a) and (b), respectively.

From these envelopes of the laser pulse, the pulse front tilt and the angular dispersion can be determined. In Fig. 2(a), the arrival time of the laser pulse, the centroid (solid line) along the time axis linearly varies across the beam, implying that the laser pulse has a constant pulse front tilt. In Fig. 2(b), $k_c(\omega)$, the centroid along the k -axis related with the signal angle, nonlinearly varies as away from the center frequency. This implies that the angular dispersion, the derivative of the $k_c(\omega)$ respect to optical frequency, is not a constant but a function of optical frequency. This is because the phase mismatch rapidly increases at the blue side of the spectrum, while it is relatively small and does not change much at the red side.

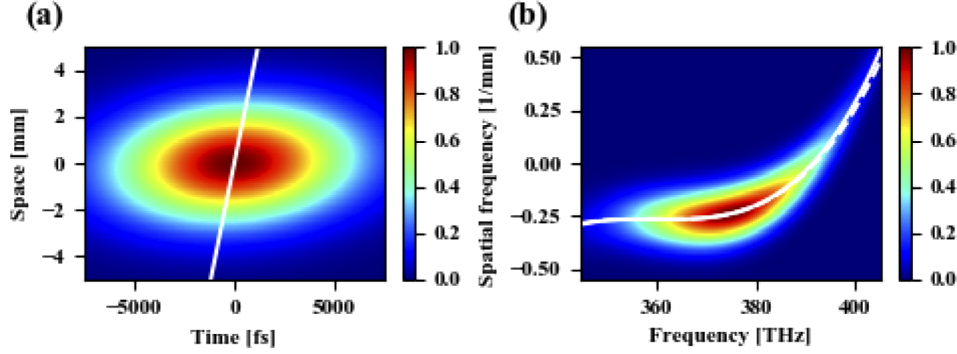


Fig. 2. (a) An envelope of the laser electric field in Eq. (28) in the x - t domain. The solid line in the x - t domain indicates the pulse front tilt. (b) An envelope of the electric field in the ω - k domain. The solid line in the ω - k domain, obtained from Eq. (32), shows the centroid of the electric field, whose derivative with respect to ω is the angular dispersion.

For extending the angular dispersion analysis by numerical Fourier transform of Eq. (28) to the ns laser pulse, the huge memory and a large computational effort are required. Therefore, an analytic analysis is rather required, but it is not easy because the Fourier transform of the exponent of the third degree polynomial or higher cannot be handled analytically. However, if the laser electric field has a large temporal chirp, $1/\beta \gg \tau_{cf}^2$, where τ_{cf} is the pulse width of a chirp-free pulse, the Fourier transform can be obtained using the following relation [36].

$$A(x, \omega = 2\beta t) = \sqrt{\frac{-i}{2\beta}} \exp[i2\beta t^2] A(x, t). \quad (31)$$

The temporal Fourier transform of the laser pulse in the x - t domain can be expressed as

$$A(x, \omega) \propto \exp\left[\frac{i\omega^2}{4\beta}\right] \exp\left[\frac{i\Delta k(\omega)}{2 \tan[\varepsilon(\omega)]} x\right]. \quad (32)$$

Using the frequency shift properties of the spatial Fourier transform, the complex amplitude in the ω - k domain is given by

$$\text{FT}_x[A(k_x, \omega)] = B\left(k_x - \frac{\Delta k(\omega)}{2 \tan[\varepsilon(\omega)]}, \omega\right), \quad (33)$$

where $B(x, \omega) = A(x, \omega) \exp[-i\Delta k(\omega)x/2 \tan[\varepsilon(\omega)]]$, and $B(k_x, \omega) = \text{FT}_x[B(x, \omega)]$. The centroid of the envelope in the ω - k domain is expressed as

$$k_c(\omega) = \frac{\Delta k(\omega)}{2 \tan \varepsilon(\omega)}. \quad (34)$$

The centroid of the envelope, Eq. (34) is plotted as the solid line, as shown in Fig. 2(b), and the solid line matches well with the envelope of the laser pulse, calculated numerically. This means

that Eq. (34) can be used to estimate the angular dispersion of the broadband laser pulse in the ns-OPCPA without the numerical Fourier transform of Eq. (30). In addition, this result indicates that the wavefront rotation is a major contributor to the angular dispersion in the ns-OPCPA whereas the pulse front tilt effect is negligible in the ns-OPCPA.

3. Experiment

3.1. Measurement of the signal angle after the OPCPA amplifier

For verifying the generation of the angular dispersion in a ns-OPCPA amplifier, the angular dispersion before and after the ns-OPCPA amplifier, placed after a ns-stretcher in the 4 PW laser at CoReLS, were measured. The experimental setup of the OPCPA amplifier and the angular dispersion measurement are shown in Fig. 3(a). After stretched to 2.5 ns by an Offner-type stretcher with the group delay dispersion of $6.3 \times 10^6 \text{ fs}^2$, a laser pulse with 20 uJ energy was injected into the OPCPA amplifier as the signal beam. The OPCPA amplifier consisted of two stages of β -barium borate (BBO) crystals. The BBO crystal lengths were 15 mm and 4 mm for the first and the second stages, respectively. The radius ($1/e^2$) of the pump and the signal beam are 2.45 mm. The shape of the signal beam is a Gaussian, and the shape of the pump beam is top-hat. When a frequency-doubled Nd:YAG laser with 800 mJ energy pumped the OPCPA amplifier, the amplified signal energies were 140 mJ and 240 mJ for the first and the second stages, respectively. Because the gain of the second stage was considerably small and the condition of Eq. (14) could not be satisfied, the effect of wavefront rotation on angular dispersion was investigated only for the first stage of the OPCPA amplifier. The detailed configuration of the OPCPA amplifier can be found in [9]. To avoid the parasitic second harmonic generation that decreases the OPCPA efficiency, the tangential phase-matching in which the pointing vector of the pump beam follows the idler beam was adopted in the OPCPA amplifier.

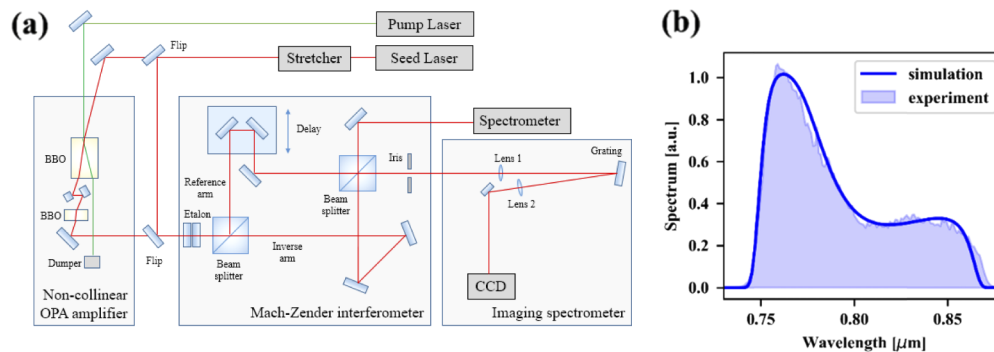


Fig. 3. (a) Schematics of the experimental setup for measuring the angular dispersion generated by the noncollinear OPCPA amplifier. (b) Measured laser spectrum (blue shaded) and calculated spectrum (blue line).

The phase-matching angle and the noncollinear angle of the OPCPA amplifier were adjusted with the consideration for the final spectrum of the 4 PW laser. The output spectrum of the OPCPA amplifier was controlled such that the laser spectrum after the final booster amplifier of the 4 PW laser became as broad as possible. As the spectral shaping process in the OPCPA amplifier, a red-side suppressed laser spectrum was prepared to compensate for the gain depletion effect in the final booster amplifier that preferentially amplifies the leading edge of a laser pulse, i.e., the red-side of a positively chirped laser pulse. As shown in Fig. 3(b), the laser spectrum was set to be significantly protruded in the blue-side by adjusting the phase-matching condition to be $\Delta k = 0$ at $\lambda = 765 \text{ nm}$. In this phase-matching condition, the amplified spectrum of the

OPCPA amplifier was measured experimentally and compared with the one obtained from the analytic method [33] in Fig. 3(b).

The diagnostic system to measure the angular dispersion was composed of an etalon, a Mach-Zehnder interferometer with image inversion [37], and an imaging spectrometer, as shown in Fig. 3(a). The etalon with a free spectral range of about 11 THz was used, and its transmission peaks within the laser spectrum were 759, 778, 800, 824, and 851 nm. The spectrally resolved fringes at the etalon transmission peaks were recorded by the imaging spectrometer, and the angular dispersion could be obtained from the measured fringe spacing. The diagnostics was based on a spectrally resolved interferometer [38], adopted because of its highest sensitivity among the angular dispersion diagnostics [39]. The diagnostic system was operated as follows: two replicas produced by the Mach-Zehnder interferometer generated a fringe pattern after being recombined, and then the fringe pattern, spectrally resolved by the gold-coated grating, was image-relayed by two lenses ($f_1 = 150$ mm, $f_2 = 125$ mm) onto a CCD camera with the magnification factor of 0.833. In the inverting arm, the laser beam image was flipped horizontally so that the fringe pattern appears with its spacing depending on the wavelength if the laser beam has the angular dispersion. The measured signal angle from fringe spacing s can be described by [38]

$$\theta_{\text{experiment}}(\lambda) = \lambda \sin[s]. \quad (35)$$

For determining the signal angle variation of each spectral beam, the wavelength-resolved fringes of the input and amplified signal for 759, 778, 800, 824, and 851 nm were measured, and they are shown in Figs. 4(a) and (b). As the fringe spacing can be easily distinguished in the Fourier space, a 1-D Fourier transform was performed with respect to the horizontal axis of the image. In the Fourier space, shown in Figs. 4(c) and (d), three vertical lines exist, and the vertical lines at both sides provide the spatial frequency of a fringe. The spatial frequency was determined after averaging the results along the vertical direction. As shown in Figs. 4(c) and (d), the spatial frequency of the ns-OPCPA output beam was wavelength-dependent, and it became reduced, as compared to the input beam. This means that the signal angle of each spectral beam changed after the ns-OPCPA amplifier due to the generation of the angular dispersion.

A comparison was made between the experimentally measured signal angle and the numerically calculated one for validating the theory on the angular dispersion in the ns-OPCPA. It is noted that in Sec. 2 theory, the angular dispersion was represented as the derivative of the centroid in the ω - k domain, not as the signal angle. Thus, for comparison, the wavelength-dependent signal angle is newly derived from Eq. (30) and it can be expressed as

$$\theta_{\text{theory}}(\lambda) = \sin^{-1} \left[\frac{k_c(\lambda)}{k} \right]. \quad (36)$$

Since the signal beam was refracted on the end surface of the nonlinear crystal in the experiment, the refraction angle by Snell's law was taken into account for calculating the signal angles after the nonlinear crystal. The measured and theoretical signal angle with respect to the wavelength is plotted in Fig. 5(a) as the blue dot and the solid red line, respectively. The measured and theoretical angular dispersion is also shown in Fig. 5(b) as the blue line and the red line, respectively, where the theoretical angular dispersion was calculated by taking the derivative of the Eq. (30), and the measured angular chirp was computed by differentiating the Lagrange polynomial, determined from the measured signal angle. The results in Fig. 5 show a good agreement between the theory and the experiment. The calculated signal angle and angular dispersion for the phase matching at 800 nm are also plotted as the dashed red lines in Fig. 5 for comparison.

3.2. Influence of the angular dispersion on focal spot parameters

Because the angular dispersion existing in an ultrahigh power laser can increase the pulse duration [40] and the focused beam size [41,42], the degradation of focal spot parameters should be

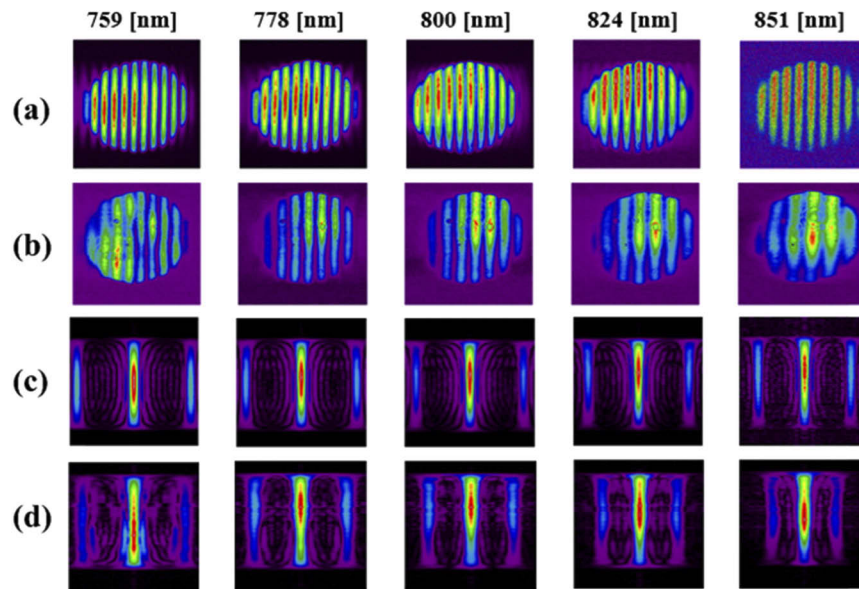


Fig. 4. Fringes of the input to the ns-OPCPA amplifier (a) and the output of the ns-OPCPA amplifier (b). The wavelengths of these images are 759, 778, 799, 824, and 851 nm from left to right. (c) and (d) 1D spatial Fourier-transformed images are represented for the images of (a) and (b), respectively.

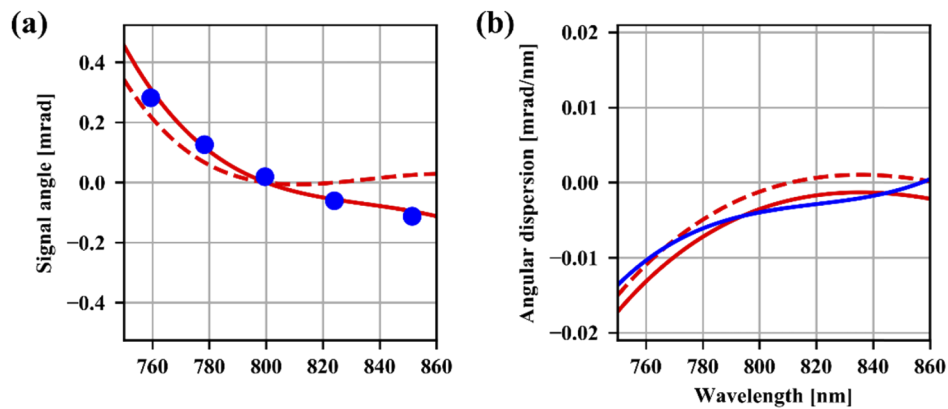


Fig. 5. (a) Measured (blue dot) and calculated (red solid line) signal angles for the experimental conditions (phase matching at 765 nm) after the nonlinear crystal. The signal angle calculated for the phase matching at 800 nm is shown as the red dashed line for comparison. (b) Measured angular dispersion of the signal beam (blue line) and calculated angular dispersion (red solid line). The calculated angular dispersions for the phase matching at 800 nm are shown as the red dashed line.

evaluated [24]. If a laser pulse does not have spatiotemporal coupling, it is sufficient to assess the performance of a beam based on its beam size and pulse duration. In case a laser pulse contains spatiotemporal couplings, focal spot parameters such as effective radius, effective pulse duration, and spatiotemporal Strehl ratio, enable to properly evaluate beam characteristics [35,43]. Effective radius is given by

$$r_{\text{eff}} = \frac{\sqrt{F(x, y)/F_0}}{\pi}, \quad (37)$$

where the fluence $F(x, y)$, and the peak fluence $F_0 = \max(F(x, y))$. The effective pulse duration is given by

$$t_{\text{eff}} = \frac{1}{P_0} \int P(t) dt, \quad (38)$$

where the power $P(t) = \iint I(x, y, t) dx dy$, and the peak power $P_0 = \max(P(t))$. The spatiotemporal Strehl ratio is defined as

$$ST_{\text{stc}} = \frac{\max(I(x, y, t))}{\max(I_0(x, y, t))}, \quad (39)$$

where I_0 is the intensity of the diffraction-limited and bandwidth-limited pulse.

To determine the focal spot parameters, the laser electric field at the focus was simulated using the amplified spectrum and the signal angle of a laser pulse, the aberration-free focus with a focusing optics of f-number 1.6, and spatially uniform pulse compression. The unidirectional pulse propagation method was used to simulate the pulse propagation from the near field to the far-field [44]. For comparison of phase matching conditions, the signal angle in the near field was considered for the cases of the experimental configuration and the zero phase mismatch at 800 nm [25]. It was also simulated to improve the focal spot parameters by reducing the angular dispersion using a prism pair [43,45] and a spatial filter [46]. The detailed results of the focal spot parameters are listed in Table 1.

Table 1. Focal spot parameters with different conditions

Parameter	Experimental condition	Zero phase mismatch at 800 nm	Prism pair	Prism pair & spatial filter	Diffraction- and bandwidth-limited
x [μm , FWHM]	4.22	2.16	1.75	1.57	1.36
y [μm , FWHM]	1.30	1.34	1.34	1.35	1.36
τ [fs, FWHM]	24.9	17.2	16.2	15.4	15.4
Strehl ratio	0.358	0.598	0.764	0.853	1.00
Effective radius r_{eff} [μm]	2.00	1.55	1.37	1.30	1.20
Effective duration τ_{eff} [fs]	49.1	32.9	26.0	22.4	19.8
Spatiotemporal Strehl ratio ST_{stc}	0.256	0.506	0.702	0.840	1.00

4. Discussion

The measurement of the signal angle clearly confirmed that the angular dispersion was induced in the ns-OPCPA amplifier. The angular dispersion of -3.97×10^{-3} mrad/nm at 800 nm, obtained by taking the derivative of the signal angle, whereas the angular dispersion of the input signal beam was measured to -0.586×10^{-3} mrad/nm at 800 nm, was close to the predicted value of -3.55×10^{-3} mrad/nm at 800 nm by Eq. (34), and it decreased rapidly as decreasing wavelength, as shown in the solid blue line in Fig. 5(b). According to the theoretical calculation, the variation of the signal angle induced by the ns-OPCPA amplifier is proportional to the phase mismatch, and measured result also shows that the signal angle changes rapidly with decreasing wavelength like phase mismatch.

Since the measured angular dispersion was small, the effect of the angular dispersion on the focal spot was evaluated and listed in Table 1. In the case of the experimental configuration, the spatiotemporal Strehl ratio at the focus could decrease to 0.256 due to the increase of the effective pulse duration by 2.5 times and the effective radius by 1.7 times. This result suggested that even small magnitude of the angular dispersion in a strongly chirped laser pulse could severely degrade the achievable laser intensity, which necessitates the control of the angular dispersion to produce near diffraction-limited and bandwidth-limited pulses.

A couple of approaches were assessed for minimizing the angular dispersion. The first approach was to obtain the zero phase mismatch at 800 nm, instead of 765 nm, because the phase mismatch can be reduced [24,25]. However, the angular dispersion still exists, as shown in the dashed red line in Fig. 5(b). In this configuration, the spatiotemporal Strehl ratio was 0.506, because the first-order term of angular dispersion was reduced. On the other hand, this method enhanced the red side of the laser spectrum, which prevents the compensation of the gain depletion effect in subsequent CPA amplifiers.

The use of external devices with the phase matching at 765 nm, such as a dispersive optical element or a spatial filter, was also examined. For the compensation of angular dispersion, a prism pair [47,48], a grating pair [49], or imaging optics with grating [50,51] can be utilized. Among the compensating methods, the compensation with prism pairs was simulated with an optimum angle obtained by the least-square method. This compensation could improve the spatiotemporal Strehl ratio by about three times. A more powerful method to reduce the angular dispersion would be the introduction of a spatial filter, which can improve the spatiotemporal coupling and other aberrations. This method is effective in cleaning the laser pulse distortion [46], but the distortion is removed at the expense of laser energy during the spatial filtering. As a method to increase the transmittance of the spatial filter, the first-order term of the angular dispersion was pre-compensated with a pair of prisms before the spatial filter. After the prism pair and the spatial filter, the focal spot parameters approaching those of the diffraction-limited and bandwidth-limited pulse could be accomplished with the spatiotemporal Strehl ratio of 0.840, when the transmitted energy of 75% is normalized to one. In the 4 PW laser, after controlling the angular dispersion, we could achieve the ultrahigh laser intensity of 5×10^{22} W/cm² [45].

5. Conclusion

We have demonstrated that the angular dispersion can be induced in the ns-OPCPA amplifier employed as the frontend of the 4 PW laser. The angular dispersion, measured precisely using a Mach-Zehnder interferometer, matches well the result of the theoretical analysis. We have found from the spatiotemporal analysis of the OPCPA amplifier that the wavefront rotation can be introduced by the phase mismatch with the spatial walk-off and the wavefront rotation leads to the angular dispersion, whereas the pulse front tilt does not affect the angular dispersion. By installing a vacuum spatial filter, the angular dispersion of the ns-OPCPA amplifier could be significantly reduced to an acceptable level to produce ultrahigh intensity laser pulses [45], paving the way to explore strong field physics at unprecedented laser intensity.

Disclosures

The authors declare no conflicts of interest.

References

1. D. Strickland and G. Mourou, "Compression of amplified chirped optical pulses," *Opt. Commun.* **56**(3), 219–221 (1985).
2. J. H. Sung, H. W. Lee, J. Y. Yoo, J. W. Yoon, C. W. Lee, J. M. Yang, Y. J. Son, Y. H. Jang, S. K. Lee, and C. H. Nam, "4.2 PW, 20 fs Ti:sapphire laser at 0.1 Hz," *Opt. Lett.* **42**(11), 2058–2061 (2017).
3. C. N. Danson, C. Haefner, J. Bromage, T. Butcher, J.-C. F. Chanteloup, E. A. Chowdhury, A. Galvanauskas, L. A. Gizzi, J. Hein, D. I. Hillier, N. W. Hopps, Y. Kato, E. A. Khazanov, R. Kodama, G. Korn, R. Li, Y. Li, J. Limpert,

- J. Ma, C. H. Nam, D. Neely, D. Papadopoulos, R. R. Penman, L. Qian, J. J. Rocca, A. A. Shaykin, C. W. Siders, C. Spindloe, S. Szatmári, R. M. G. M. Trines, J. Zhu, P. Zhu, and J. D. Zuegel, "Petawatt and exawatt class lasers worldwide," *High Power Laser Sci. Eng.* **7**, e54 (2019).
4. A. Macchi, M. Borghesi, and M. Passoni, "Ion acceleration by superintense laser-plasma interaction," *Rev. Mod. Phys.* **85**(2), 751–793 (2013).
 5. W. P. Leemans, B. Nagler, A. J. Gonsalves, C. Toth, K. Nakamura, C. G. R. Geddes, E. Esarey, C. B. Schroeder, and S. M. Hooker, "GeV electron beams from a centimetre-scale accelerator," *Nat. Phys.* **2**(10), 696–699 (2006).
 6. M. D. Perry, D. Pennington, B. C. Stuart, G. Tietbohl, J. A. Britten, C. Brown, S. Herman, B. Golick, M. Kartz, J. Miller, H. T. Powell, M. Vergino, and V. Yanovsky, "Petawatt laser pulses," *Opt. Lett.* **24**(3), 160–162 (1999).
 7. M. Aoyama, K. Yamakawa, Y. Akahane, J. Ma, N. Inoue, H. Ueda, and H. Kiriya, "0.85-PW, 33-fs Ti:sapphire laser," *Opt. Lett.* **28**(17), 1594–1596 (2003).
 8. J. H. Sung, S. K. Lee, T. J. Yu, T. M. Jeong, and J. Lee, "0.1 Hz 1.0 PW Ti:sapphire laser," *Opt. Lett.* **35**(18), 3021–3023 (2010).
 9. H. W. Lee, Y. G. Kim, J. Y. Yoo, J. W. Yoon, J. M. Yang, H. Lim, C. H. Nam, J. H. Sung, and S. K. Lee, "Spectral shaping of an OPCPA preamplifier for a sub-20-fs multi-PW laser," *Opt. Express* **26**(19), 24775–24783 (2018).
 10. I. N. Ross, P. Matousek, M. Towrie, A. J. Langley, and J. L. Collier, "The prospects for ultrashort pulse duration and ultrahigh intensity using optical parametric chirped pulse amplifiers," *Opt. Commun.* **144**(1-3), 125–133 (1997).
 11. D. N. Papadopoulos, P. Ramirez, K. Genevri, L. Ranc, N. Lebas, A. Pellegrina, C. Le Blanc, P. Monot, L. Martin, J. P. Zou, F. Mathieu, P. Audebert, P. Georges, and F. Druon, "High-contrast 10 fs OPCPA-based front end for multi-PW laser chains," *Opt. Lett.* **42**(18), 3530–3533 (2017).
 12. H. Kiriya, N. Inoue, Y. Akahane, and K. Yamakawa, "Prepulse-free, multi-terawatt, sub-30-fs laser system," *Opt. Express* **14**(1), 438–445 (2006).
 13. A. Bayramian, J. Armstrong, G. Beer, R. Campbell, B. Chai, R. Cross, A. Erlandson, Y. Fei, B. Freitas, R. Kent, J. Menapace, W. Molander, K. Schaffers, C. Siders, S. Sutton, J. Tassano, S. Telford, C. Ebberts, J. Caird, and C. Barty, "High-average-power femto-petawatt laser pumped by the Mercury laser facility," *J. Opt. Soc. Am. B* **25**(7), B57–B61 (2008).
 14. J. Rothhardt, S. Demmler, S. Hädrich, T. Peschel, J. Limpert, and A. Tünnermann, "Thermal effects in high average power optical parametric amplifiers," *Opt. Lett.* **38**(5), 763–765 (2013).
 15. S. Demmler, J. Rothhardt, S. Hädrich, J. Bromage, J. Limpert, and A. Tünnermann, "Control of nonlinear spectral phase induced by ultra-broadband optical parametric amplification," *Opt. Lett.* **37**(19), 3933–3935 (2012).
 16. X. Liang, X. Xie, J. Kang, Q. Yang, H. Wei, M. Sun, and J. Zhu, "Design and experimental demonstration of a high conversion efficiency OPCPA pre-amplifier for petawatt laser facility," *High Power Laser Sci. Eng.* **6**, e58 (2018).
 17. I. Ahmad, S. A. Trushin, Z. Major, C. Wandt, S. Klingebiel, T. J. Wang, V. Pervak, A. Popp, M. Siebold, F. Krausz, and S. Karsch, "Frontend light source for short-pulse pumped OPCPA system," *Appl. Phys. B* **97**(3), 529–536 (2009).
 18. E. Hugonnot, G. Deschaseaux, O. Hartmann, and H. Coic, "Design of PETAL multipetawatt high-energy laser front end based on optical parametric chirped pulse amplification," *Appl. Opt.* **46**(33), 8181–8187 (2007).
 19. C. Dorrer, A. Consentino, D. Irwin, J. Qiao, and J. D. Zuegel, "OPCPA front end and contrast optimization for the OMEGA EP kilojoule, picosecond laser," *J. Opt.* **17**(9), 094007 (2015).
 20. H. Yoshida, E. Ishii, H. Okita, R. Kodama, H. Fujita, Y. Kitagawa, N. Miyanaga, Y. Izawa, and T. Yamanaka, "Study on OPCPA front-end system for PW laser," in *Summaries of Papers Presented at the Lasers and Electro-Optics., CLEO '02, Technical Digest., (IEEE, 2002)*, 402–403.
 21. A. Shirakawa, I. Sakane, and T. Kobayashi, "Pulse-front-matched optical parametric amplification for sub-10-fs pulse generation tunable in the visible and near infrared," *Opt. Lett.* **23**(16), 1292–1294 (1998).
 22. S. Akturk, X. Gu, P. Gabolde, and R. Trebino, "The general theory of first-order spatio-temporal distortions of Gaussian pulses and beams," *Opt. Express* **13**(21), 8642–8661 (2005).
 23. S. Akturk, X. Gu, E. Zeek, and R. Trebino, "Pulse-front tilt caused by spatial and temporal chirp," *Opt. Express* **12**(19), 4399–4410 (2004).
 24. J. Bromage, C. Dorrer, and J. D. Zuegel, "Angular-dispersion-induced spatiotemporal aberrations in noncollinear optical parametric amplifiers," *Opt. Lett.* **35**(13), 2251–2253 (2010).
 25. A. Giree, M. Mero, G. Arisholm, M. J. J. Vrakking, and F. J. Furch, "Numerical study of spatiotemporal distortions in noncollinear optical parametric chirped-pulse amplifiers," *Opt. Express* **25**(4), 3104–3121 (2017).
 26. O. Isaienko and E. Borguet, "Pulse-front matching of ultrabroadband near-infrared noncollinear optical parametric amplified pulses," *J. Opt. Soc. Am. B* **26**(5), 965–972 (2009).
 27. A. Zaukevičius, V. Jukna, R. Antipenkov, V. Martinėnaitė, A. Varanavičius, A. P. Piskarskas, and G. Valiulis, "Manifestation of spatial chirp in femtosecond noncollinear optical parametric chirped-pulse amplifier," *J. Opt. Soc. Am. B* **28**(12), 2902–2908 (2011).
 28. I. N. Ross, J. L. Collier, P. Matousek, C. N. Danson, D. Neely, R. M. Allot, D. A. Pepler, C. Hernandez-Gomez, and K. Osvay, "Generation of terawatt pulses by use of optical parametric chirped pulse amplification," *Appl. Opt.* **39**(15), 2422–2427 (2000).
 29. E. W. Gaul, M. Martinez, J. Blakeney, A. Jochmann, M. Ringuette, D. Hammond, T. Borger, R. Escamilla, S. Douglas, W. Henderson, G. Dyer, A. Erlandson, R. Cross, J. Caird, C. Ebberts, and T. Ditmire, "Demonstration of a 1.1 petawatt laser based on a hybrid optical parametric chirped pulse amplification/mixed Nd:glass amplifier," *Appl. Opt.* **49**(9), 1676–1681 (2010).

30. M. Born and E. Wolf, *Principles of optics: electromagnetic theory of propagation, interference and diffraction of light* (Elsevier, 2013).
31. J. Hebling, "Derivation of the pulse front tilt caused by angular dispersion," *Opt. Quantum Electron.* **28**(12), 1759–1763 (1996).
32. J.-C. Diels and W. Rudolph, *Ultrashort laser pulse phenomena* (Elsevier, 2006).
33. R. Baumgartner and R. Byer, "Optical parametric amplification," *IEEE J. Quantum Electron.* **15**(6), 432–444 (1979).
34. I. N. Ross, P. Matousek, G. H. C. New, and K. Osvay, "Analysis and optimization of optical parametric chirped pulse amplification," *J. Opt. Soc. Am. B* **19**(12), 2945–2956 (2002).
35. J. Bromage, J. Rothhardt, S. Hadrich, C. Dorrer, C. Joher, S. Demmler, J. Limpert, A. Tunnermann, and J. D. Zuegel, "Analysis and suppression of parasitic processes in noncollinear optical parametric amplifiers," *Opt. Express* **19**(18), 16797–16808 (2011).
36. A. Andrianov, A. Szabo, A. Sergeev, A. Kim, V. Chvykov, and M. Kalashnikov, "Computationally efficient method for Fourier transform of highly chirped pulses for laser and parametric amplifier modeling," *Opt. Express* **24**(23), 25974–25982 (2016).
37. K. Igarashi, D. Souma, K. Takeshima, and T. Tsuritani, "Selective mode multiplexer based on phase plates and Mach-Zehnder interferometer with image inversion function," *Opt. Express* **23**(1), 183–194 (2015).
38. K. Varjú, A. Kovács, G. Kurdi, and K. Osvay, "High-precision measurement of angular dispersion in a CPA laser," *Appl. Phys. B* **74**(S1), s259–s263 (2002).
39. M. Gstalter, A. Börzsönyi, and K. Osvay, "Comparison of Linear Methods for Angular Dispersion Measurement," in *2015 European Conference on Lasers and Electro-Optics - European Quantum Electronics Conference*, (Optical Society of America, 2015), CF_P_21.
40. S. Q. Zeng, D. R. Li, X. H. Lv, J. Liu, and Q. M. Luo, "Pulse broadening of the femtosecond pulses in a Gaussian beam passing an angular disperser," *Opt. Lett.* **32**(9), 1180–1182 (2007).
41. G. Pretzler, A. Kasper, and K. J. Witte, "Angular chirp and tilted light pulses in CPA lasers," *Appl. Phys. B* **70**(1), 1–9 (2000).
42. D. R. Li, X. H. Lv, S. Q. Zeng, and Q. M. Luo, "Beam spot size evolution of Gaussian femtosecond pulses after angular dispersion," *Opt. Lett.* **33**(2), 128–130 (2008).
43. A. S. Pirozhkov, Y. Fukuda, M. Nishiuchi, H. Kiriya, A. Sagisaka, K. Ogura, M. Mori, M. Kishimoto, H. Sakaki, N. P. Dover, K. Kondo, N. Nakani, K. Huang, M. Kanasaki, K. Kondo, and M. Kando, "Approaching the diffraction-limited, bandwidth-limited Petawatt," *Opt. Express* **25**(17), 20486–20501 (2017).
44. M. Kolesik, J. V. Moloney, and M. Mlejnek, "Unidirectional optical pulse propagation equation," *Phys. Rev. Lett.* **89**(28), 283902 (2002).
45. J. W. Yoon, C. Jeon, J. Shin, S. K. Lee, H. W. Lee, I. W. Choi, H. T. Kim, J. H. Sung, and C. H. Nam, "Achieving the laser intensity of 5.5×10^{22} W/cm² with a wavefront-corrected multi-PW laser," *Opt. Express* **27**(15), 20412–20420 (2019).
46. M. Miranda, M. Kotur, P. Rudawski, C. Guo, A. Harth, A. L'Huillier, and C. L. Arnold, "Spatiotemporal characterization of ultrashort laser pulses using spatially resolved Fourier transform spectrometry," *Opt. Lett.* **39**(17), 5142–5145 (2014).
47. K. Osvay, A. P. Kovacs, Z. Heiner, G. Kurdi, J. Klebniczki, and M. Csatari, "Angular dispersion and temporal change of femtosecond pulses from misaligned pulse compressors," *IEEE J. Sel. Top. Quantum Electron.* **10**(1), 213–220 (2004).
48. B. A. Richman, S. E. Bisson, R. Trebino, E. Sidick, and A. Jacobson, "Efficient broadband second-harmonic generation by dispersive achromatic nonlinear conversion using only prisms," *Opt. Lett.* **23**(7), 497–499 (1998).
49. I. Sela, "Complex grating for compensating non-uniform angular dispersion," (Google Patents, 2002).
50. T. J. Wang, Z. Major, I. Ahmad, S. A. Trushin, F. Krausz, and S. Karsch, "Ultra-broadband near-infrared pulse generation by noncollinear OPA with angular dispersion compensation," *Appl. Phys. B* **100**(1), 207–214 (2010).
51. Z. Heiner, V. Petrov, G. Steinmeyer, M. J. J. Vrakking, and M. Mero, "100-kHz, dual-beam OPA delivering high-quality, 5-cycle angular-dispersion-compensated mid-infrared idler pulses at 3.1," *Opt. Express* **26**(20), 25793–25804 (2018).